

---

# CP-PINNs: CHANGEPOINTS DETECTION IN PDES USING PHYSICS INFORMED NEURAL NETWORKS WITH TOTAL-VARIATION PENALTY

---

**Zhikang Dong**

**Paweł Polak**

Department of Applied Mathematics and Statistics  
Stony Brook University  
Stony Brook, NY, 11794, USA  
{zhikang.dong.1, pawel.polak}@stonybrook.edu

## ABSTRACT

We consider the inverse problem for the Partial Differential Equations (PDEs) such that the parameters of the dependency structure can exhibit random changepoints over time. This can arise, for example, when the physical system is either under malicious attack (e.g., hacker attacks on power grids and internet networks) or subject to extreme external conditions (e.g., weather conditions impacting electricity grids or large market movements impacting valuations of derivative contracts). For that purpose, we employ Physics Informed Neural Networks (PINNs)—universal approximators that can incorporate prior information from any physical law described by a system of PDEs. This prior knowledge acts in the training of the neural network as a regularization that limits the space of admissible solutions and increases the correctness of the function approximation. We show that when the true data generating process exhibits changepoints in the PDE dynamics, this regularization can lead to a complete miss-calibration and a failure of the model. Therefore, we propose an extension of PINNs using a Total-Variation penalty which accommodates (multiple) changepoints in the PDE dynamics. These changepoints can occur at random locations over time, and they are estimated together with the solutions. We propose an additional refinement algorithm that combines changepoints detection with a reduced dynamic programming method that is feasible for the computationally intensive PINNs methods, and we demonstrate the benefits of the proposed model empirically using examples of different equations with changes in the parameters. In case of no changepoints in the data, the proposed model reduces to the original PINNs model. In the presence of changepoints, it leads to improvements in parameter estimation, better model fitting, and a lower training error compared to the original PINNs model.

## 1 Introduction

Deep learning, and machine learning methods are widely studied and used in academia and industry, e.g., [1, 2, 3]. They perform successfully in tasks such as dimensionality reduction [4], computer vision [5], and time series analysis [6]. More recently, deep learning models have shown the ability to approximate a majority of nonlinear functions in the context of complex dynamical systems [7, 8, 9]. [10] introduced Physics Informed Neural Networks (PINNs)—an artificial intelligence approach that is suitable for solving PDEs and for solving inverse problems via data-driven discovery of the system dynamics for a given class of PDEs. Compared with traditional numerical methods [11, 12, 13], PINNs allow to solve supervised learning tasks while respecting any given law of physics described by general nonlinear PDEs. They utilize neural networks as general estimators and encode any underlying physical laws as prior information. PINNs have been widely applied in many fields, such as optics [14], cardiology [15], and power system [16].

There are many different formulations of PINNs, e.g., Physics-informed generative adversarial networks [17] which have stochastic differential equations induced generators to tackle very high dimensional problems; [18] rewrite PDEs

as backward stochastic differential equations and designs the gradient of the solution as policy function, which is approximated by deep neural networks. In reinforcement learning, [19] propose a Bayesian neural network as the prior for PDEs and use Hamiltonian Monte Carlo and variational inference as the estimator of the posterior, resulting in more accurate prediction and no overfitting.

Although PINNs are considered universal approximators, they cannot properly capture dynamics with steep slopes, singularities, and sharpe changes. Based on Petrov-Galerkin method, the hp-variational PINNs (hp-VPINNs) [20] is an extension of PINNs method that allows for localized parameters estimation with given test functions via domain decomposition. The hp-VPINNs generate a global approximation to the weak solution of the PDE with local learning algorithm that uses a domain decomposition which is preselected by the user. This leads to high accuracy of the solution.

For dynamical nonlinear system analysis, even if the law is explicitly known, there are possible discrepancies (nonlinear frictions, wind resistance, etc.) between the model and the real-world dynamics which can lead to significant deviations from the true, measured behavior. [21] propose an algorithm to identify and eliminate these discrepancies by using a sparse identification algorithm that includes an  $\ell_1$  penalty term in the PINNs loss function.

The hp-VPINNs accommodate local domain decomposition but the solution is still described by a given PDE system and the user needs to know where is the rapid change in the dynamics in order to optimally decompose the domain prior to estimation. One open problem is how to use PINNs methods in the presence of unknown changepoints in a dynamical system. Many fields have taken advantage of changepoints detection methods, e.g., [22] show how changepoint detection algorithms work on video-based surveillance. [23, 24] propose changepoints detection methods to distinguish gaps between silence, sentences, and noise in speech recognition. In medicine, changepoints detection methods are used to find heart issues in real-time monitoring [25, 26]. These methods can also detect disturbances and determine their geographic location in large-scale power grids [27]. [28] show how changepoints detection methods can analyze anomalies and attacks in the computer networks.

We introduced a changepoints detection method for the PINNs model based on total variation penalty as in [29, 30]. This technique extends PINNs to the case of continuous time dynamical systems with breakpoints by endowing loss function with an additional regularization term similar to [21]. The proposed two-step algorithm, first detects candidates for the changepoints locations, then a reduced dynamic programming step searches through the list of these candidates and estimates PINNs between them to provide the best domain decomposition and the corresponding domain specific solutions. Our CP-PINNs model, in case of no changepoints in the data, reduces to the original PINNs model, and as shown in the empirical results below, when changepoints are present in the data, it substantially outperforms the original PINNs approach.

The rest of the paper is organized as following. Section 2 gives an overview of our methodology to detect changepoints locations and estimate the unknown parameters. In Section 3 we consider the 1D advection-diffusion Equations and 2D Navier-Stokes Equations as examples to illustrate our approach. Section 4 gives extensions and ideas for future work. Section 5 concludes.

## 2 Model and Estimation

We consider a general form of parameterized and nonlinear continuous partial equations with breakpoints

$$u_t + \mathcal{N}[u; \lambda(t)] = 0, \quad (1)$$

where  $(\mathbf{x}, t) \in \Omega \times (0, T]$ ,  $\Omega \subset \mathbb{R}^d$  is the bounded domain,  $\mathcal{N}[\cdot; \lambda(t)]$  is a nonlinear operator parameterized by a function  $\lambda(t)$ , and  $u(\mathbf{x}, t)$  denotes the latent solution to the above equation. Regarding the function  $\lambda(t)$ , we make the following assumption

**Assumption 2.1.** *The function  $\lambda(t) : [0, T] \rightarrow \mathbb{R}$  is piecewise-constant, bounded, with a finite but unknown number of discontinuities  $k^*$ , located at some of the observations, i.e.,  $\lambda(t) = \sum_{i=1}^{k^*} \lambda_i \mathbf{1}_{[t_{i-1}, t_i)}(t)$ , for  $0 = t_0 < t_1 < \dots < t_{k^*} < T$ .*

### 2.1 Physics-Informed Neural Network

Following [10], in order to approximate the true solution of the PDE in (1) we use the neural network approximation  $u_{NN}(\mathbf{x}, t; \mathbf{W}, \mathbf{b})$  given by

$$u_{NN}(\mathbf{x}, t; \mathbf{W}, \mathbf{b}) = g \circ T^{(\ell)} \circ T^{(\ell-1)} \circ \dots \circ T^{(1)}(\mathbf{x}).$$

For each hidden layer, the nonlinear operator  $T^{(i)}(\mathbf{x}) = \sigma(\mathbf{W}_i \mathbf{x} + \mathbf{b}_i)$  with weights  $\mathbf{W}_i \in \mathbb{R}^{\mathcal{N}_i \times \mathcal{N}_{i-1}}$  and biases  $\mathbf{b}_i \in \mathbb{R}^{\mathcal{N}_i}$ , where  $\mathcal{N}_0 = d$  is the input dimension and in the output layer, the operator  $g : \mathbb{R}^{\mathcal{N}_\ell} \rightarrow \mathbb{R}$  is a linear activation

function. Next, define a feature function

$$f(\mathbf{x}, t) = u_t + \mathcal{N}[u; \lambda(t)],$$

and the corresponding boundary and initial residual functions

$$\begin{aligned} r_b(u_{NN}, \mathbf{x}, t) &= u_{NN} - u, & \forall (\mathbf{x}, t) \in \partial\Omega \times (0, T] \\ r_0(u_{NN}, \mathbf{x}, t) &= u_{NN} - u_0, & \forall (\mathbf{x}, t) \in \Omega \times \{t = 0\}. \end{aligned}$$

Averaging over observations on their domains, we obtain the fitting loss function for the training of the model

$$L^f = \frac{1}{N_b} \sum_{i=1}^{N_b} |r_b(\mathbf{x}_b^i, t_b^i)|^2 + \frac{1}{N_0} \sum_{i=1}^{N_0} |r_0(\mathbf{x}_0^i)|^2. \quad (2)$$

Similarly, for the observations inside the domain, the structure loss is defined as

$$L^s = \frac{1}{N} \sum_{i=1}^N |f_{NN}(\mathbf{x}^i, t^i)|^2. \quad (3)$$

Gathering together these two loss functions we obtain the total loss for the training of the model.

Standard PINNs model assumes  $\lambda(t) \equiv \lambda$  for all  $t \in [0, T]$ . In order to accommodate Assumption 2.1 in the estimation process we need to introduce additional regularization for the changes in  $\lambda(t)$ . For that purpose we use a total variation penalty on the first difference in  $\lambda(t)$ .

## 2.2 Total Variation Regularization

Let

$$V^\lambda = \sum_{i=1}^{T-1} \delta(t^i) |\Delta\lambda(t^i)|, \quad (4)$$

where  $\Delta\lambda(t^i) = \lambda(t^{i+1}) - \lambda(t^i)$ , and  $\delta(t)$  is a U-shape linear function of  $t$  which increases the penalty strength closer to the edges in order to avoid estimation instabilities around the edge (in the experiments below we use  $\delta(t) = \sqrt{\frac{T}{T-t}}$ ).

We define our loss function

$$L = L^f + L^s + V^\lambda, \quad (5)$$

where the last term is a sparsity inducing penalty similar to one used in [29] for changepoints detection in linear models. The third term in (5) is zero whenever the corresponding  $\lambda$  is constant, and it has positive values for  $i$  corresponding to changepoint location.

Training of the PINNs model uses a backpropagation algorithm on the computational graph of the problem, and it requires a differentiable loss function. In our case  $V^\lambda$  is a nondifferentiable function, and it cannot be included into the objective function in a current form. Hence, we rewrite (4) as a differentiable function which is a sum of two variables. In particular, we apply rectified linear activation (ReLU) function to  $\Delta\lambda(t)$  and  $-\Delta\lambda(t)$ , respectively, and we call them a positive part  $\Delta\lambda^+(t)$ , and a negative part  $\Delta\lambda^-(t)$ , such that

$$\begin{aligned} \Delta\lambda^+(t^i) &= \begin{cases} \Delta\lambda(t^i), & \text{for } \Delta\lambda(t^i) > 0 \\ 0, & \text{otherwise} \end{cases} \\ \Delta\lambda^-(t^i) &= \begin{cases} 0, & \text{for } \Delta\lambda(t^i) \geq 0 \\ -\Delta\lambda(t^i), & \text{otherwise.} \end{cases} \end{aligned}$$

So, the regularization term in the loss function (5) can be written as

$$V^\lambda = \sum_{i=1}^{T-1} \delta(i) [\Delta\lambda^+(t^i) + \Delta\lambda^-(t^i)]. \quad (6)$$

### 2.3 Two-Step Estimation Algorithm

Given a maximum number of changepoints  $k^*$ , a standard method of changepoints detection involves the analysis of all possible breakpoints locations that minimize the loss computed on the corresponding segments of the data. In the context of our model, such a problem would correspond to the objective function of the form

$$\arg \min_{t_0 < \dots < t_{k^*}} \sum_{k=1}^{k^*} (L^f + L^s)(\{\mathbf{x}^i, t^i\}_{i=t_{k-1}+1}^{t_k}), \quad (7)$$

where  $t_0, \dots, t_{k^*}$  are changepoints locations selected from all possible partitions of the data and for each of the partitions the corresponding PINNs model would have to be estimated to evaluate the loss function (7). If the computational complexity of the PINNs method is  $\mathcal{P}$ , a naive approach to the problem above would require a  $O(2^n \mathcal{P})$  computations. Dynamic programming (DP) provides a computationally more efficient way of solving this minimization problem, and it has a time complexity of  $O(k^* n^2 \mathcal{P})$ . This is still too large for the PINNs algorithm to run on a realistic dataset.

Our CP-PINNs approach is an enhanced version of the DP method which combines two steps. First, we run PINNs with total variation penalty included in the loss function (5), where  $V^\lambda$  is given in (6). This gives us a set of candidates for the changepoints locations. Second, we run a DP step but instead of considering all possible segmentations of the data, we consider only the segmentations based on the changepoint candidates from the first step candidates. This greatly reduces the computational time to  $O((1 + k^{*3})\mathcal{P})$  which is much lower than the original DP method because  $k^* \ll n$ , and it makes the two-step CP-PINNs approach feasible—especially with small  $k^*$ .

In the first step, in order to select changepoints candidates we need to detect large changes in the estimated  $\lambda(t)$ . In order to do so, we plot  $\log |\Delta \hat{\lambda}(t)|^{-1}$  estimated using PINNs model with total variation penalty as in the loss function (5) and select the largest negative peaks in the series as our candidates for the changepoints.

## 3 Experiment Results

All of the experiments below are trained 100,000 times with Adam [31] optimizer and 50,000 times with Limited-memory BFGS [32] optimizer. The model is deployed on a single NVIDIA GeForce RTX 3080 Ti graphics card.

### 3.1 Advection-Diffusion Equation

As the first example, we discuss the advection-diffusion equation, which is widely used in heat transfer [33], mass transfer [34], and fluid dynamics problems [35]. The equation of one-dimensional form is given by

$$\begin{aligned} \frac{\partial u}{\partial t} + v \frac{\partial u}{\partial x} &= \kappa \frac{\partial^2 u}{\partial x^2} \\ u(t, -1) = u(t, 1) &= 0 \\ u(x, 0) &= -\sin(\pi x), \end{aligned}$$

where  $v$  is the advection coefficient and  $\kappa$  is the diffusivity coefficient,  $u(x, t) : \Omega \rightarrow \mathbb{R}$ , and  $\Omega = [-1, 1] \times [0, 1]$ . [36] has given the analytical solution of the advection-diffusion equations by using infinite series summation. In our cases, we assume that advection coefficient  $v = 1$  is fixed, and changepoints are only associated with diffusivity coefficients.

Without loss of generality, we use the same number of observations on the boundary and for the initial conditions in the two terms (2) and (3), respectively.

Our neural network has 3 hidden layers, each of them has five neurons and use  $\tanh()$  activation function. We generate 500 points over space interval  $[-1, 1]$ , and set 101 equally spaced time steps in the  $[0, 1]$  interval, so the total observations are 50500. The initial value of diffusivity coefficients  $\kappa(t)$  is sampled from a normal distribution with mean 0 and standard deviation 1.

#### 3.1.1 One breakpoint with balanced time intervals

In this case, the velocity coefficient is fixed to be a constant  $v = 1$  and the diffusion coefficient  $\kappa(t)$  is a piecewise constant function of time with one breakpoint, where  $\kappa_1 = 1$  on  $[0, 0.5)$  and  $\kappa_2 = 0.05$  on  $[0.5, 1]$ .

The results are shown in Figure 1. The model finds the true breakpoint which is the middle point of the time interval. And estimation of the edge is stable.

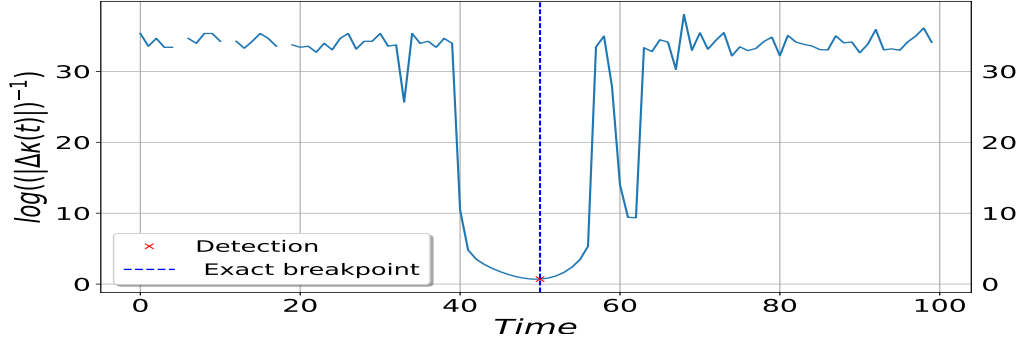


Figure 1: One breakpoint with balanced time intervals for 1D advection-diffusion equation. The true breakpoint is at interval 50 and the detected one is also at interval 50. The  $x$  axis is time and  $y$  axis is  $\log(|\Delta\hat{\kappa}(t)|^{-1})$ .

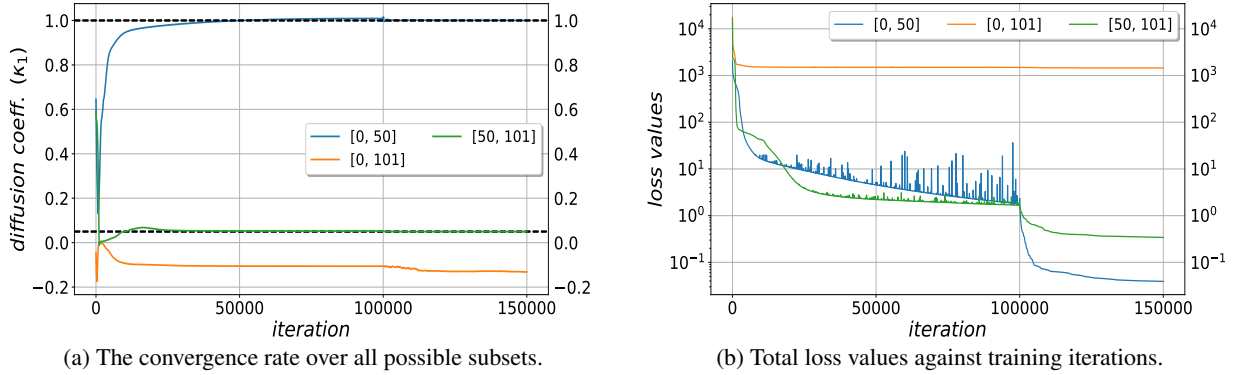


Figure 2: One breakpoint with balanced time intervals. The parameter estimation on interval  $[0, 50)$ ,  $[0, 100]$  and  $(50, 100]$  are 1.0004,  $-0.1316$  and 0.0498. The training errors are 0.0391, 1453.6112, and 0.3420 respectively.

For the detected change point  $t^* = 0.5$ , we train PINNs on each candidate and compare estimation results. The results are shown in Figure 2. We find that the parts before and after the breakpoint converge to their corresponding diffusion coefficient very quickly. We exclude the negative estimation results because it does not make sense in this PDE.

We display the exact solution of the dynamic system and estimated solution of each subset in Figure 3. The estimated solution is very close to the true functions. When compared with the PINNs model estimated without any changepoints on the whole time domain. The PINNs fit is much worst—see Figure 2 (b) for the corresponding total loss in the training iterations.

### 3.1.2 Two breakpoints with balanced time intervals

In general, we might have multiple breakpoints in the dynamics. The same technique can be applied in this situation. We use the same neural network structure and settings as in the example above. We assume there are two breakpoints, where  $\kappa_1 = \kappa_3 = 1$  on  $[0, 0.33)$  and  $[0.66, 1]$ , and  $\kappa_2 = 0.05$  on  $[0.33, 0.66)$ . We also adjust the height of peaks to control the number of candidates. The results are shown in Figure 4. The estimation of edges is still stable.

The two detected positions are 0.33 and 0.68, which are very close to the real change points locations. Subsequently, we train distinct neural networks on all possible subsets. Figure 5 shows that the models training on  $[0, 0.33)$ ,  $[0.33, 0.68)$  and  $[0.68, 1]$  yield the best estimation results. On the contrary, those training on any intervals containing breakpoints are unable to produce the correct diffusion coefficient and have much higher loss function values.

In Figure 6, we show the real solution of the whole dynamic system and the estimated solution of all possible subsets.

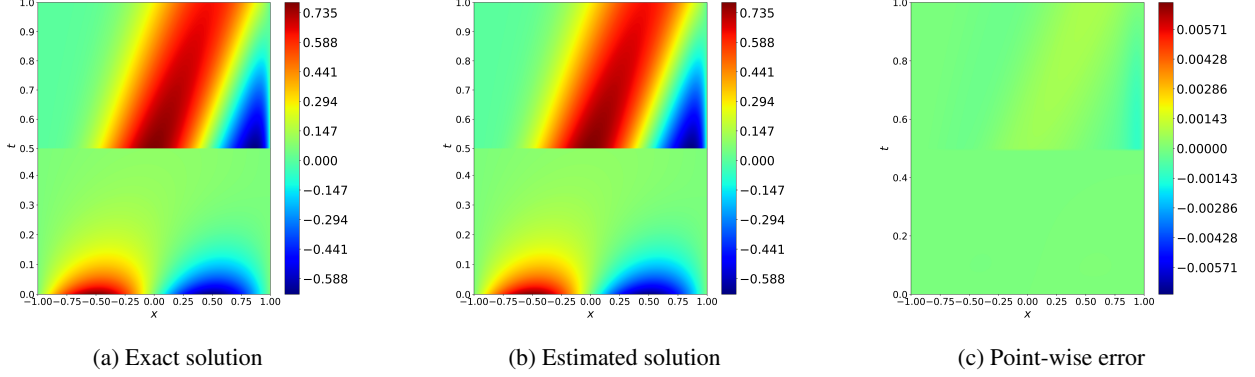


Figure 3: The solution of dynamical systems with one balanced breakpoint.

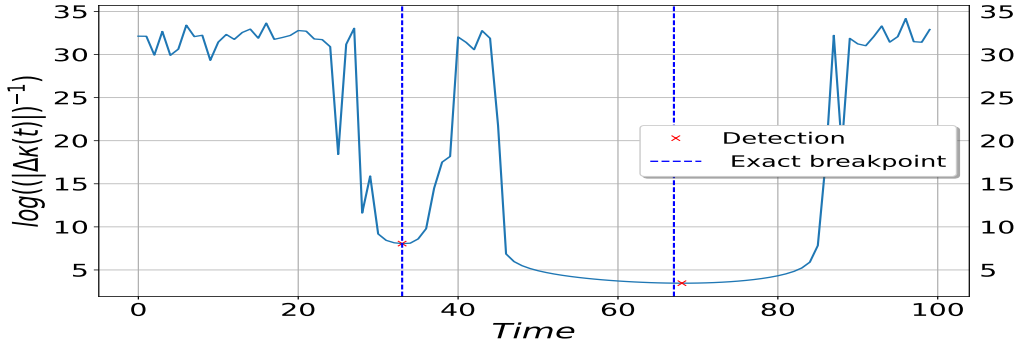


Figure 4: Two breakpoints with balanced time intervals for 1D advection-diffusion equation. The true breakpoints are at interval 33 and 66, and the candidate points are at interval 33 and 68.

### 3.1.3 One breakpoint with imbalanced time intervals

In the case of imbalanced data, where the breakpoint appears closer to the edge, our model still can detect it. We set  $\kappa_1 = 1$  on  $[0, 0.2)$  and  $\kappa_2 = 0.05$  on  $[0.2, 1]$ . The model detects the changepoint at 0.19.

The results are shown in Figure 7. Figure 8 shows the training process on each potential candidate. And the comparison between estimated solutions and exact solutions are shown in Figure 9.

## 3.2 2D Navier-Stokes Equations

In another experiment, we detect changepoints among the parameters of 2D Navier-Stokes equations. Namely,

$$\begin{aligned} u_t + (uu_x + vv_y) &= -p_x + \lambda(t)(u_{xx} + u_{yy}) \\ v_t + (uv_x + vv_y) &= -p_y + \lambda(t)(v_{xx} + v_{yy}), \end{aligned} \quad (8)$$

for  $u(x, y, t)$ ,  $v(x, y, t)$  and  $p(x, y, t) : \Omega \rightarrow \mathbb{R}$ , where  $\Omega = [-5, 10] \times [-5, 5] \times [0, T]$ . The two functions  $u(x, y, t)$  and  $v(x, y, t)$  denote the stream-wise and transverse velocity components, respectively, and the third function  $p(t, x, y)$  is the measurement of fluid pressure. In our experiment, we focus on incompressible fluid flow passing through the 2D circular cylinder with radius = 0.5.  $\lambda$  is the viscosity coefficient, where  $\lambda = \frac{1}{Re}$ .  $Re$  is the Reynolds number, where  $Re = UD/\nu$ .  $U$  is the velocity scale,  $D$  is the length scale and  $\nu$  is the kinematic viscosity.

Following [10], we expect that solutions of (8) are divergence free functions, thus we have

$$\frac{\partial u}{\partial x} + \frac{\partial v}{\partial y} = 0. \quad (9)$$

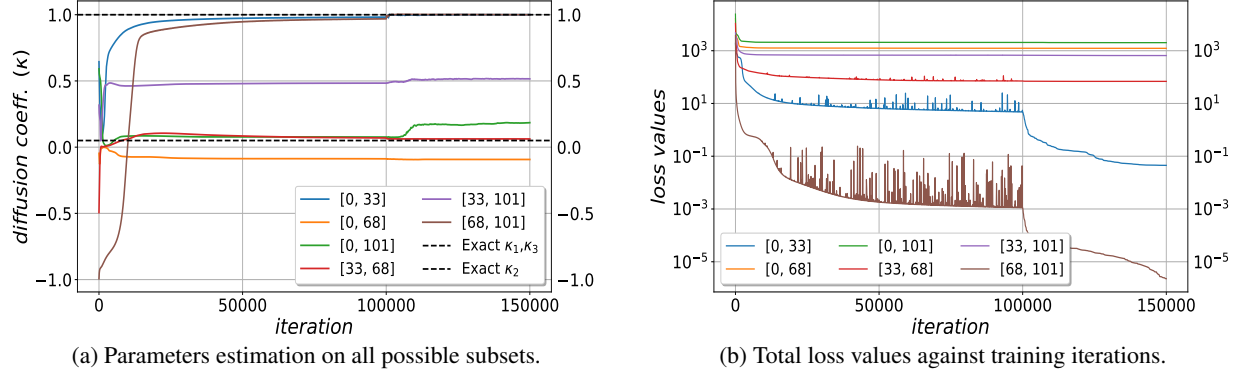


Figure 5: Two breakpoints with balanced time intervals. The parameter estimation on interval  $[0, 0.33]$ ,  $[0.33, 0.68]$  and  $[0.68, 1]$  are 1.0003, 0.0620, 1.0000. Training errors are 0.0451, 68.8005, and  $2.27 \times 10^{-6}$ .

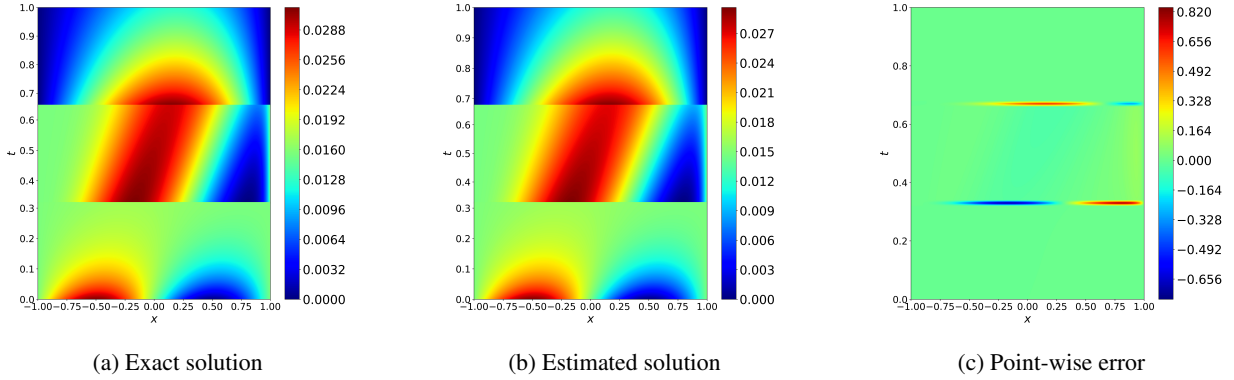


Figure 6: The solution of 1D advection-equation with two balanced breakpoints.

In order to satisfy (9), one would assume hidden functions  $\psi(x, y, t)$ , where

$$u = \frac{\partial \psi}{\partial y}, \quad v = -\frac{\partial \psi}{\partial x}.$$

Moreover, one needs to define feature functions:

$$f = \frac{\partial u}{\partial t} + \left( u \frac{\partial u}{\partial x} + v \frac{\partial u}{\partial y} \right) + \frac{\partial p}{\partial x} - \lambda(t) \left( \frac{\partial^2 u}{\partial x^2} + \frac{\partial^2 u}{\partial y^2} \right)$$

$$g = \frac{\partial v}{\partial t} + \left( u \frac{\partial v}{\partial x} + v \frac{\partial v}{\partial y} \right) + \frac{\partial p}{\partial y} - \lambda(t) \left( \frac{\partial^2 v}{\partial x^2} + \frac{\partial^2 v}{\partial y^2} \right).$$

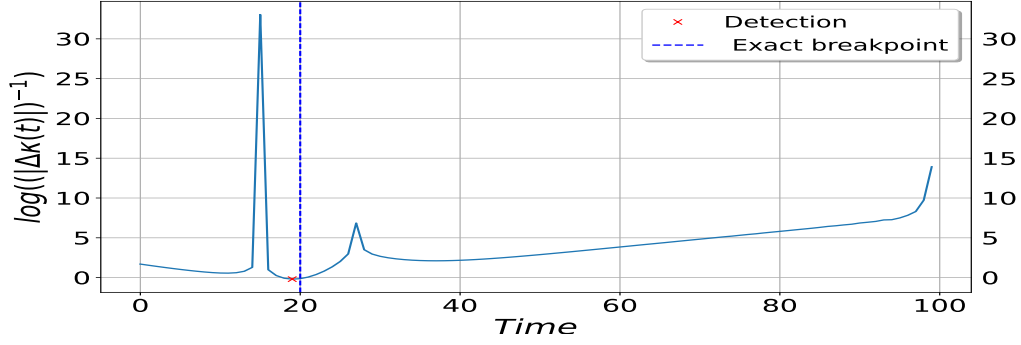


Figure 7: One breakpoint with imbalanced time intervals for 1D advection-diffusion equation. The true breakpoint is at interval 20 and the detected one is at interval 19.

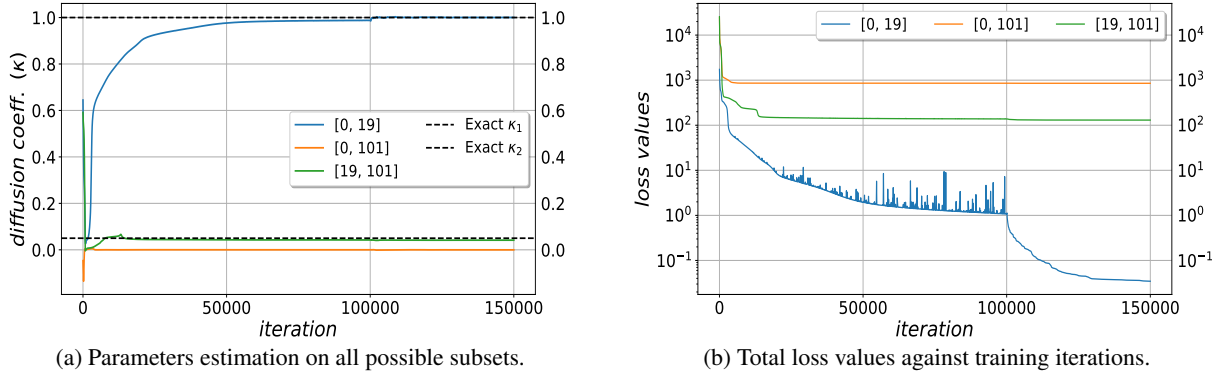


Figure 8: One breakpoint with imbalanced time intervals. The parameter estimation on interval  $[0, 19]$ ,  $[0, 101]$  and  $[19, 101]$  are 1.0003,  $-0.0001$  and 0.0415. The training errors are 0.0346, 853.0608, and 130.1135 respectively.

Compared with the 1D case, the two terms in the loss function, (2) and (3), have two components each

$$L_{(u)}^f = \frac{1}{N} \sum_{i=1}^N |u_{NN}(x_i, y_i, t_i) - u(x_i, y_i, t_i)|^2$$

$$L_{(v)}^f = \frac{1}{N} \sum_{i=1}^N |v_{NN}(x_i, y_i, t_i) - v(x_i, y_i, t_i)|^2$$

$$L_{(f)}^s = \frac{1}{N} \sum_{i=1}^N |f_{NN}(x_i, y_i, t_i)|^2$$

$$L_{(g)}^s = \frac{1}{N} \sum_{i=1}^N |g_{NN}(x_i, y_i, t_i)|^2.$$

Thus the corresponding loss function is defined as

$$L = L_{(u)}^f + L_{(v)}^f + L_{(f)}^s + L_{(g)}^s + V^\lambda.$$

Following the experiment in [37], the data for our analysis is generated using the following boundary conditions: no-slip conditions on the cylinder surface; far-field with Dirichlet boundary conditions:  $(u, v) = (1, 0)$  at the bottom and top boundaries; the Dirichlet boundary condition:  $(u, v) = (1, 0)$  at the left boundary for corresponding inflow; and the flow moves out of the right boundary with fixed pressure  $p = 0$ .



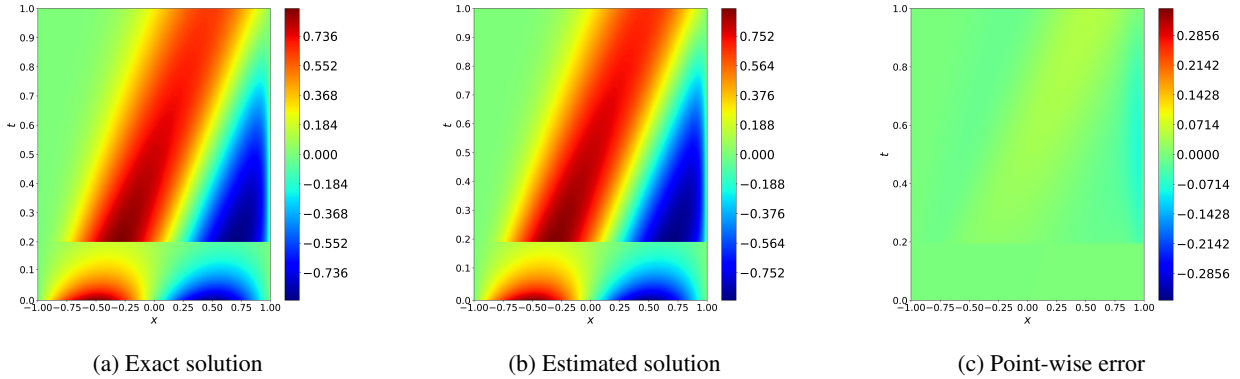


Figure 9: The solution of dynamical systems with one imbalanced breakpoint.

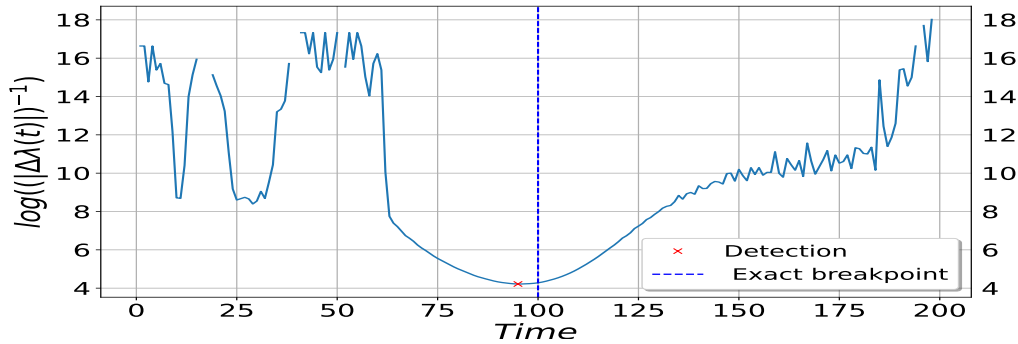


Figure 10: One breakpoint with balanced time intervals for 2D Navier-Stokes equations. The true breakpoint is at interval 100 and the detected one is at interval 95. The  $x$  axis is time and  $y$  axis is  $\log \left| \Delta \hat{\lambda}(t) \right|^{-1}$ .

For this experiment, our neural network structure is composed of 8 hidden layers with 20 neurons in each layer and the  $\tanh()$  as activation function. We have created a training dataset by randomly sub-sampling the high-resolution dataset, which is generated by four order piecewise polynomial finite element solver as in [38]. In order to show the ability of our method to detect changepoints and learn parameters from dynamic systems with sparse training data, we choose 700 points from the 2D surface, corresponding to a mere 9% of the total available.

### 3.2.1 One breakpoint with balanced time intervals

We consider the 2D Navier-Stokes equations as in (8) with the viscosity coefficient  $\lambda(t)$  as a piecewise constant function of time with one breakpoint, where  $\lambda_1 = 0.5$  on  $[0, 2)$  and  $\lambda_2 = 0.02$  on  $[2, 4]$ . The results are shown in Figure 10. In order to shorten training time, we set an early stopping tolerance: the difference between 1.0 and the next smallest representable float larger than 1.0. For 64-bit binary floats in the IEEE-754 standard, this value is  $2^{-52}$ . Consequently, not all training would reach the maximum 150,000 iterations. The corresponding results are shown in Figure 11.

Mean square error and parameter estimation error on each candidate interval are shown in Table 1. Again, our CP-PINNs model provides much more accurate estimates than the original PINNs model estimated on the entire time interval.

### 3.2.2 Two breakpoints with balanced time intervals

We also consider the example that there are two breakpoints in the dynamical system, and their locations are evenly distributed. In this example,  $t \in [0, 6]$ , and we have 300 equally spaced time steps in total. For time intervals  $[0, 100)$  and  $[200, 300]$ , we generate data by using  $\lambda_1 = \lambda_3 = 0.5$ , and we use  $\lambda_2 = 0.01$  to generate data on time interval  $[100, 200)$ .

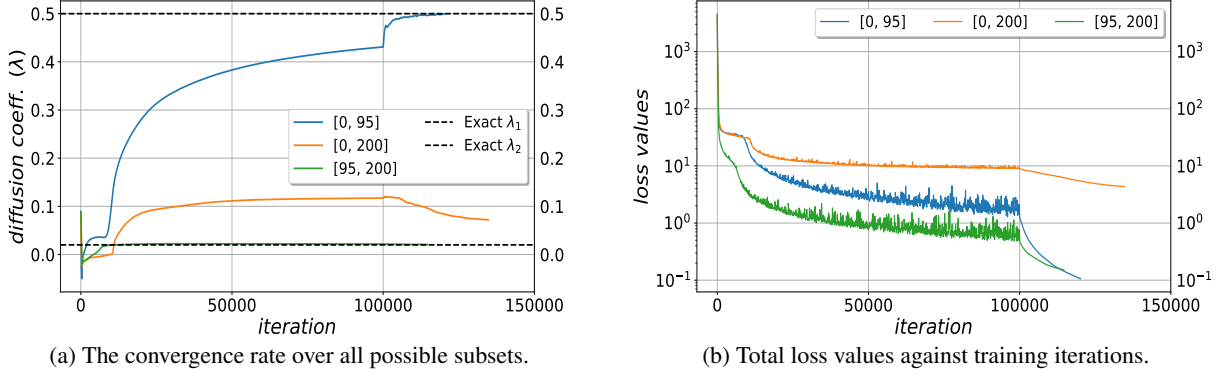


Figure 11: One breakpoint with balanced time intervals. The parameter estimation on  $[0, 95]$ ,  $[0, 200]$  and  $(95, 200]$  are 0.4989, 0.0719 and 0.0208, respectively. The training errors on these intervals are 0.1061, 4.3442, and 0.1520 respectively.

Interval	MSE of u	MSE of v	Error of $\lambda$
$[0, 95)$	0.000006	0.000004	0.214571%
$[0, 200]$	0.000396	0.000263	172.489518%
$(95, 200]$	0.000016	0.000009	8.420763%

Table 1: Mean squared error of stream-wise velocity, traverse velocity and parameter estimation error on each potential candidates with one balanced breakpoint.

The training results are shown in Figure 12. For the DP step, we have 3 changepoints candidates with 10 possible partitions. We estimate the viscosity parameter on each subinterval. All the training results are shown in Figure 13. Table 2 shows the mean square errors and parameter estimation errors on all potential intervals.

### 3.2.3 One breakpoint with imbalanced time intervals

We also give the example of one change point with imbalanced time intervals for Navier-Stokes equations. Here  $t \in [0, 2.7]$ , and we have 135 equally spaced time steps in this case. We use  $\lambda_1 = 0.5$  and  $\lambda_2 = 0.02$  to generate training data, and the change happens at time step 100. We estimate the breakpoint location at 93 which is very close to real breakpoint. The results are shown in Figure 14. We also estimate parameters in each time interval, the results are shown in Figure 15. We show the mean square error of solutions and the estimation error of  $\lambda$  on every potential interval. The results are shown in Table 3.

Interval	MSE of u	MSE of v	Error of $\lambda$
$[0, 92)$	0.000015	0.000007	0.467032%
$[0, 98)$	0.000007	0.000004	0.202596%
$[0, 201)$	0.000657	0.000375	415.000422%
$[0, 300]$	0.000625	0.000359	879.713949%
$[92, 98)$	0.000017	0.000013	100.384215%
$[92, 201)$	0.000028	0.000020	18.714501%
$[92, 300]$	0.000742	0.000473	952.496209%
$[98, 201)$	0.000007	0.000003	4.879582%
$[98, 300]$	0.000808	0.000406	1080.164707%
$[201, 300]$	0.000015	0.000008	0.859374%

Table 2: Mean squared error of stream-wise velocity, traverse velocity and parameter estimation error on each potential candidates with two balanced breakpoints.

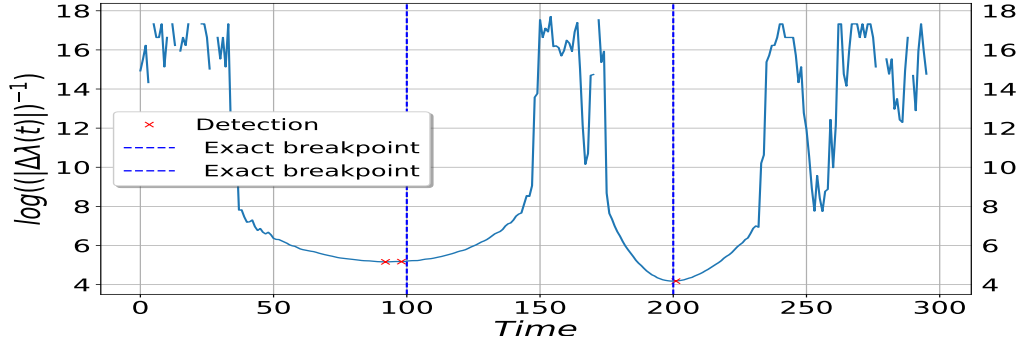


Figure 12: Two breakpoints with balanced time intervals for 2D Navier-Stokes equations. The true breakpoints are at interval 100 and 200. And the potential candidates are found at 92, 98 and 201.

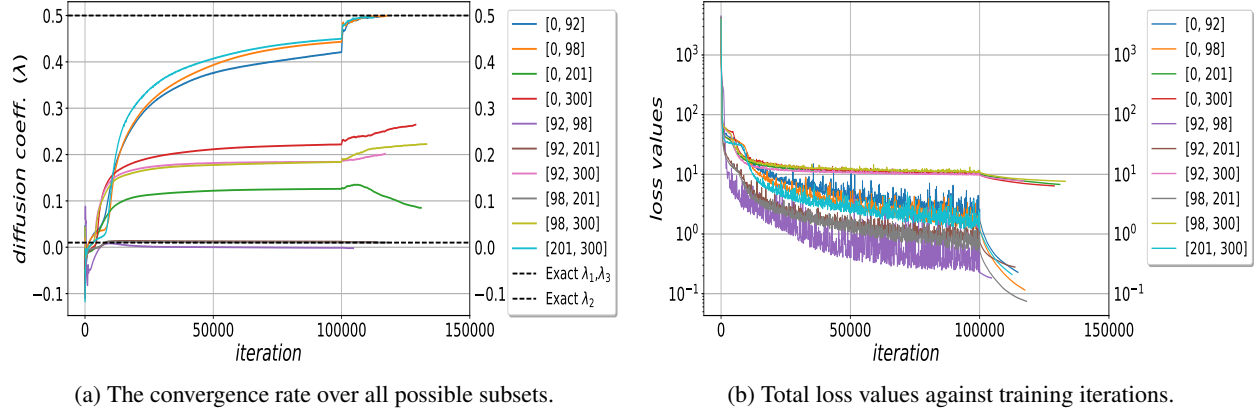


Figure 13: Two breakpoints with balanced time intervals. The parameter estimation for interval  $[0, 98)$ ,  $[98, 201)$  and  $[201, 300]$  are 0.4990, 0.0102 and 0.4957. The corresponding training errors are 0.1153, 0.0745 and 0.2097, respectively.

## 4 Discussion

Assumption 2.1 can be modified to allow, e.g., for piecewise linear  $\lambda(t)$  function. In that case, similarly to [39] one should replace the total variation penalty (4) with the second order difference penalty  $|\Delta^2 \lambda(t^i)| = |\Delta \lambda(t^{i+1}) - \Delta \lambda(t^i)|$  to induce sparsity in the changes of the slope of the estimated  $\lambda(t)$  function. One can also consider  $\ell_2$  regularization on the differences in  $\lambda(t)$  to capture smooth changes in the function.

Another assumption that we made in our analysis so far is that the observations are equally spaced. We can extend our method to data which is irregularly spaced. First, consider the estimation of the underlying continuous function  $\lambda(t)$

Interval	MSE of u	MSE of v	Error of $\lambda$
$[0, 93)$	0.000013	0.000008	0.250596%
$[0, 135]$	0.000169	0.000117	516.275559%
$[93, 135]$	0.000015	0.000010	34.152066%

Table 3: Mean squared error of stream-wise velocity, traverse velocity and parameter estimation error on each potential candidates with one imbalanced breakpoints.

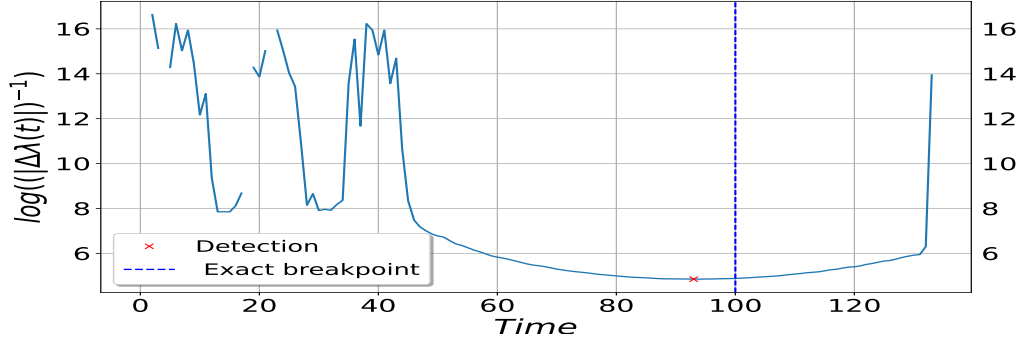
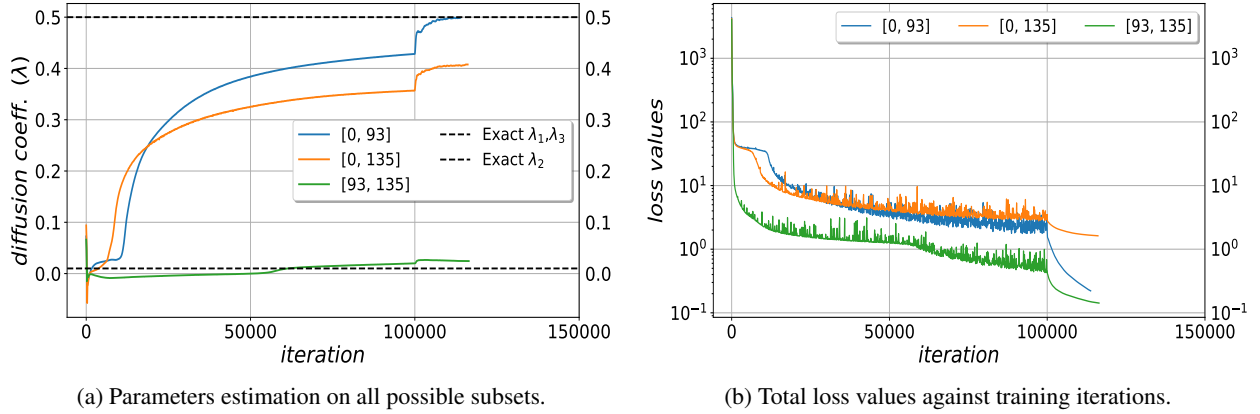


Figure 14: One breakpoint with imbalanced time intervals for 2D Navier-Stokes equations. The true breakpoint is at interval 100 and the detected one is at interval 93.



(a) Parameters estimation on all possible subsets.

(b) Total loss values against training iterations.

Figure 15: One breakpoint with imbalanced time intervals. The parameter estimation on interval  $[0, 93)$ ,  $[0, 135]$  and  $[93, 135]$  are 0.4987, 0.4077 and 0.0244, respectively.

from a finite number of data points. The total variation regularization term in a continuous form can be written as

$$\int_0^T \delta(t) |\Delta\lambda(t)| dt.$$

This can be simplified by using the standard interpolation problem as explained in [39]. In particular, we can write

$$\sum_{i=1}^{n-1} \delta(t_i) \left| \frac{\lambda(t_{i+1}) - \lambda(t_i)}{t_{i+1} - t_i} \right|.$$

From the optimal points  $\lambda(t_i)$ ,  $i = 1, \dots, n$ , we can recover the solution to the original piecewise constant problem: the piecewise-constant function, for  $\lambda^*(t_i)$ , given by

$$\lambda^*(t) = \frac{t_{i+1} - t}{t_{i+1} - t_i} \lambda^*(t_i),$$

for  $i = 1, \dots, n$ , is the optimal piecewise constant  $\lambda(t)$ .

Finally, one can consider a more general problem with changepoints in the spatio-temporal domain, i.e.,  $\lambda(t, \mathbf{x})$  as a function of time and space. The regularization term then would include increments across time and the neighboring observations. Such a regularization would be considerably more difficult to incorporate in the estimation process and so far it has been only considered for the linear models, see [40].

## 5 Conclusion

We propose a new method to detect changepoints in the dynamic systems described by general PDE dynamics. Our algorithm consists of two-steps: The first step is to allow for a general model with time-varying parameters and total variation regularization on the first order difference of unknown piecewise constant parameters and detect candidates for the changepoints. The second step is a reduced DP step which trains PINNs on all of the potential subdomains from the first step. In case of no changepoints in the data, the method reduces to the original PINNs approach. In case of changepoints present in the data, we show that we can detect changepoints accurately and capture the patterns of the dynamic system much better than applying PINNs on the whole domain.

## References

- [1] Ian Goodfellow, Yoshua Bengio, and Aaron Courville. *Deep learning*. MIT press, 2016.
- [2] Yann LeCun, Yoshua Bengio, and Geoffrey Hinton. Deep learning. *nature*, 521(7553):436–444, 2015.
- [3] Alex Krizhevsky, Ilya Sutskever, and Geoffrey E Hinton. Imagenet classification with deep convolutional neural networks. *Advances in neural information processing systems*, 25, 2012.
- [4] Diederik P Kingma and Max Welling. Auto-encoding variational bayes. *arXiv preprint arXiv:1312.6114*, 2013.
- [5] Christian Szegedy, Vincent Vanhoucke, Sergey Ioffe, Jon Shlens, and Zbigniew Wojna. Rethinking the inception architecture for computer vision. In *Proceedings of the IEEE conference on computer vision and pattern recognition*, pages 2818–2826, 2016.
- [6] Klaus Greff, Rupesh K Srivastava, Jan Koutník, Bas R Steunebrink, and Jürgen Schmidhuber. Lstm: A search space odyssey. *IEEE transactions on neural networks and learning systems*, 28(10):2222–2232, 2016.
- [7] Hrushikesh N Mhaskar and Tomaso Poggio. Function approximation by deep networks. *arXiv preprint arXiv:1905.12882*, 2019.
- [8] Bethany Lusch, J Nathan Kutz, and Steven L Brunton. Deep learning for universal linear embeddings of nonlinear dynamics. *Nature communications*, 9(1):1–10, 2018.
- [9] Ingrid Daubechies, Ronald DeVore, Simon Foucart, Boris Hanin, and Guergana Petrova. Nonlinear approximation and (deep) ReLU networks. *Constructive Approximation*, 55(1):127–172, 2022.
- [10] Maziar Raissi, Paris Perdikaris, and George E Karniadakis. Physics-informed neural networks: A deep learning framework for solving forward and inverse problems involving nonlinear partial differential equations. *Journal of Computational Physics*, 378:686–707, 2019.
- [11] Markus Bär, Rainer Hegger, and Holger Kantz. Fitting partial differential equations to space-time dynamics. *Physical Review E*, 59(1):337, 1999.
- [12] Thorsten G Müller and Jens Timmer. Fitting parameters in partial differential equations from partially observed noisy data. *Physica D: Nonlinear Phenomena*, 171(1-2):1–7, 2002.
- [13] Xiaolei Xun, Jiguo Cao, Bani Mallick, Arnab Maity, and Raymond J Carroll. Parameter estimation of partial differential equation models. *Journal of the American Statistical Association*, 108(503):1009–1020, 2013.
- [14] Yuyao Chen, Lu Lu, George Em Karniadakis, and Luca Dal Negro. Physics-informed neural networks for inverse problems in nano-optics and metamaterials. *Optics express*, 28(8):11618–11633, 2020.
- [15] Francisco Sahli Costabal, Yibo Yang, Paris Perdikaris, Daniel E Hurtado, and Ellen Kuhl. Physics-informed neural networks for cardiac activation mapping. *Frontiers in Physics*, 8:42, 2020.
- [16] George S Misyris, Andreas Venzke, and Spyros Chatzivasileiadis. Physics-informed neural networks for power systems. In *2020 IEEE Power & Energy Society General Meeting (PESGM)*, pages 1–5. IEEE, 2020.
- [17] Liu Yang, Dongkun Zhang, and George Em Karniadakis. Physics-informed generative adversarial networks for stochastic differential equations. *SIAM Journal on Scientific Computing*, 42(1):A292–A317, 2020.
- [18] Jiequn Han, Arnulf Jentzen, and Weinan E. Solving high-dimensional partial differential equations using deep learning. *Proceedings of the National Academy of Sciences*, 115(34):8505–8510, 2018.
- [19] Liu Yang, Xuhui Meng, and George Em Karniadakis. B-pinns: Bayesian physics-informed neural networks for forward and inverse pde problems with noisy data. *Journal of Computational Physics*, 425:109913, 2021.
- [20] Ehsan Kharazmi, Zhongqiang Zhang, and George Em Karniadakis. hp-vpinns: Variational physics-informed neural networks with domain decomposition. *Computer Methods in Applied Mechanics and Engineering*, 374:113547, 2021.

- [21] Kadierdan Kaheman, Eurika Kaiser, Benjamin Strom, J Nathan Kutz, and Steven L Brunton. Learning discrepancy models from experimental data. *arXiv preprint arXiv:1909.08574*, 2019.
- [22] Richard J Radke, Srinivas Andra, Omar Al-Kofahi, and Badrinath Roysam. Image change detection algorithms: a systematic survey. *IEEE transactions on image processing*, 14(3):294–307, 2005.
- [23] Md Foezur Rahman Chowdhury, S-A Selouani, and D O’Shaughnessy. Bayesian on-line spectral change point detection: a soft computing approach for on-line asr. *International Journal of Speech Technology*, 15(1):5–23, 2012.
- [24] David Rybach, Christian Gollan, Ralf Schluter, and Hermann Ney. Audio segmentation for speech recognition using segment features. In *2009 IEEE International Conference on Acoustics, Speech and Signal Processing*, pages 4197–4200. IEEE, 2009.
- [25] M Staudacher, S Telser, A Amann, H Hinterhuber, and M Ritsch-Martel. A new method for change-point detection developed for on-line analysis of the heart beat variability during sleep. *Physica A: Statistical Mechanics and its Applications*, 349(3-4):582–596, 2005.
- [26] Ping Yang, Guy Dumont, and John Mark Ansermino. Adaptive change detection in heart rate trend monitoring in anesthetized children. *IEEE transactions on biomedical engineering*, 53(11):2211–2219, 2006.
- [27] Zekun Yang, Yu Chen, Ning Zhou, Aleksey Polunchenko, and Yilu Liu. Data-driven online distributed disturbance location for large-scale power grids. *IET Smart Grid*, 2(3):381–390, 2019.
- [28] Alexander G Tartakovsky. Rapid detection of attacks in computer networks by quickest changepoint detection methods. In *Data analysis for network cyber-security*, pages 33–70. World Scientific, 2014.
- [29] Zaid Harchaoui and Céline Lévy-Leduc. Multiple change-point estimation with a total variation penalty. *Journal of the American Statistical Association*, 105(492):1480–1493, 2010.
- [30] Zaid Harchaoui, Eric Moulines, and Francis Bach. Kernel change-point analysis. *Advances in neural information processing systems*, 21, 2008.
- [31] Diederik P Kingma and Jimmy Ba. Adam: A method for stochastic optimization. *arXiv preprint arXiv:1412.6980*, 2014.
- [32] Dong C Liu and Jorge Nocedal. On the limited memory bfgs method for large scale optimization. *Mathematical programming*, 45(1):503–528, 1989.
- [33] Seyed Ali Hosseini, Nasser Darabiha, and Dominique Thévenin. Lattice boltzmann advection-diffusion model for conjugate heat transfer in heterogeneous media. *International Journal of Heat and Mass Transfer*, 132:906–919, 2019.
- [34] Ronbanchob Apiratikul. Application of analytical solution of advection-dispersion-reaction model to predict the breakthrough curve and mass transfer zone for the biosorption of heavy metal ion in a fixed bed column. *Process Safety and Environmental Protection*, 137:58–65, 2020.
- [35] Ailian Chang, HongGuang Sun, Chunmiao Zheng, Bingqing Lu, Chengpeng Lu, Rui Ma, and Yong Zhang. A time fractional convection–diffusion equation to model gas transport through heterogeneous soil and gas reservoirs. *Physica A: Statistical Mechanics and its Applications*, 502:356–369, 2018.
- [36] Abdelkader Mojtabi and Michel O Deville. One-dimensional linear advection–diffusion equation: Analytical and finite element solutions. *Computers & Fluids*, 107:189–195, 2015.
- [37] Chris D Cantwell, David Moxey, Andrew Comerford, Alessandro Bolis, Gabriele Rocco, Gianmarco Mengaldo, Daniele De Grazia, Sergey Yakovlev, J-E Lombard, Dirk Ekelschot, et al. Nektar++: An open-source spectral/hp element framework. *Computer physics communications*, 192:205–219, 2015.
- [38] David Moxey, Chris D Cantwell, Yan Bao, Andrea Cassinelli, Giacomo Castiglioni, Sehun Chun, Emilia Juda, Ehsan Kazemi, Kilian Lackhove, Julian Marcon, et al. Nektar++: Enhancing the capability and application of high-fidelity spectral/hp element methods. *Computer Physics Communications*, 249:107110, 2020.
- [39] Seung-Jean Kim, Kwangmoo Koh, Stephen Boyd, and Dimitry Gorinevsky.  $\ell_1$  trend filtering. *SIAM review*, 51(2):339–360, 2009.
- [40] Yu-Xiang Wang, James Sharpnack, Alex Smola, and Ryan Tibshirani. Trend Filtering on Graphs. In Guy Lebanon and S. V. N. Vishwanathan, editors, *Proceedings of the Eighteenth International Conference on Artificial Intelligence and Statistics*, volume 38 of *Proceedings of Machine Learning Research*, pages 1042–1050, San Diego, California, USA, 09–12 May 2015. PMLR.